Check for updates

LASER & PHOTONICS REVIEWS
www.lpr-journal.org

Anomalous Intensity Quenching of Resonant Raman Scattering in Atomically Thin MoS_2

Rui Mei, Yang-Guang Zhong, Jia-Liang Xie, Jiang-Bin Wu, Wen-Na Du, Xin-Hui Zhang, Xin-Feng Liu, Miao-Ling Lin, and Ping-Heng Tan**

Resonance Raman scattering (RRS) is widely recognized for dramatically enhancing the intensity of Raman modes through the precise tuning of excitation energy to be resonant with the electronic transition energy in semiconductors. However, this work reports that in monolayer MoS_2 flake (1LM), when the excitation energy is resonant with the A-exciton energy, the A_1' and E' modes exhibit anomalous quenching of the Raman intensity, which is even comparable to that under the non-resonant condition. This unusually weakened resonant Raman intensity is ascribed to the band filling effect (BFE) caused by the photoexcited carriers at the band edges, which obstructs the Raman scattering pathway related to the band-edge states. Notably, this quenched Raman intensity can be recovered by introducing non-radiative relaxation channels of interfacial charge transfer in 1LM-based heterostructures and intervalley scattering in multilayer MoS_2 to mitigate the BFE. As the BFE is widely present in low-dimensional semiconductors, this work paves a potential approach to manipulate Raman intensity enhancement by controlling carrier relaxation dynamics in low-dimensional semiconductors and related heterostructures.

1. Introduction

Raman scattering is highly favored as an efficient tool for probing various elementary excitations (e.g., phonon) and their interactions (e.g., electron-phonon interaction) in both bulk and low-dimensional materials.[1–5] For a first-order Raman scattering process involving a phonon with zero wavevector ($q = 0$), the incident light first excites electron from the initial state i into an intermediate state m by creating an electron-hole pair; then the electron or hole is scattered by a phonon with $q = 0$ into an intermediate state m' and finally the electron-hole pair recombines by radiating energy-shifted photons.[6] When a specific real electronic state participates in the Raman scattering pathway as an intermediate state m (m'), Raman intensity is expected to be significantly enhanced, which is known as the incoming (outgoing) resonance Raman scattering (RRS)(**Figure 1a**).[6–8] RRS has been widely employed to study electronic transitions and electron–phonon coupling with enhanced sensitivity and selectivity.[9–13]

Transition metal dichalcogenides (TMDs) host a rich variety of exciton states,[14] including the K-valley-derived A exciton (with transition energy E_A) and B exciton,[15–17] along with the C exciton resulting from van Hove singularities,[18] making them ideal platforms for RRS studies. For instance, in monolayer MoS_2 (1LM), the intralayer A_1' and E' modes exhibit strong enhancement when the excitation energy (E_{ex}) matches the transition energy of the C exciton (E_C), enabling in-depth studies of strain and doping effects.[8,14] Moreover, a comprehensive understanding of the E_A-related RRS mechanism provides critical insights into exciton-phonon coupling and advances optoelectronic applications. In principle, the remarkably high joint density of A-exciton state creates ideal conditions for promising resonant Raman enhancement. However, the inherent direct bandgap characteristic enables intense photoluminescence under the resonance with E_A, overwhelming the Raman signal. Consequently, a comprehensive understanding of E_A-related RRS and the underlying exciton-phonon interactions has remained elusive, hindering progress in fundamental studies and device engineering.

In this study, we observe that when E_{ex} is in resonance with E_A of 1LM, $I(A_1')$ is roughly one-tenth of its value under the C-exciton resonance ($E_{ex} \approx E_C$), whereas in monolayer WS_2, the corresponding $I(A_1')$ is twice that under its C-exciton resonance.[12] The extremely weak resonant Raman intensity in 1LM obtained under E_A resonance condition indicates that a significant quenching effect occurs. This is attributed to the blocking of scattering pathways due to the band filling effect (BFE), which arises

R. Mei, J.-L. Xie, J.-B. Wu, X.-H. Zhang, M.-L. Lin, P.-H. Tan
State Key Laboratory of Semiconductor Physics and Chip Technologies
Institute of Semiconductors
Chinese Academy of Sciences
Beijing 100083, China
E-mail: linmiaoling@semi.ac.cn; phtan@semi.ac.cn
R. Mei, J.-L. Xie, J.-B. Wu, X.-H. Zhang, M.-L. Lin, P.-H. Tan
Center of Materials Science and Optoelectronics Engineering
University of Chinese Academy of Sciences
Beijing 100049, China
Y.-G. Zhong, W.-N. Du, X.-F. Liu
CAS Key Laboratory of Standardization and Measurement for Nanotechnology
National Center for Nanoscience and Technology
Beijing 100190, China
The ORCID identification number(s) for the author(s) of this article can be found under https://doi.org/10.1002/lpor.202500821

DOI: 10.1002/lpor.202500821

 © 2025 Wiley-VCH GmbH

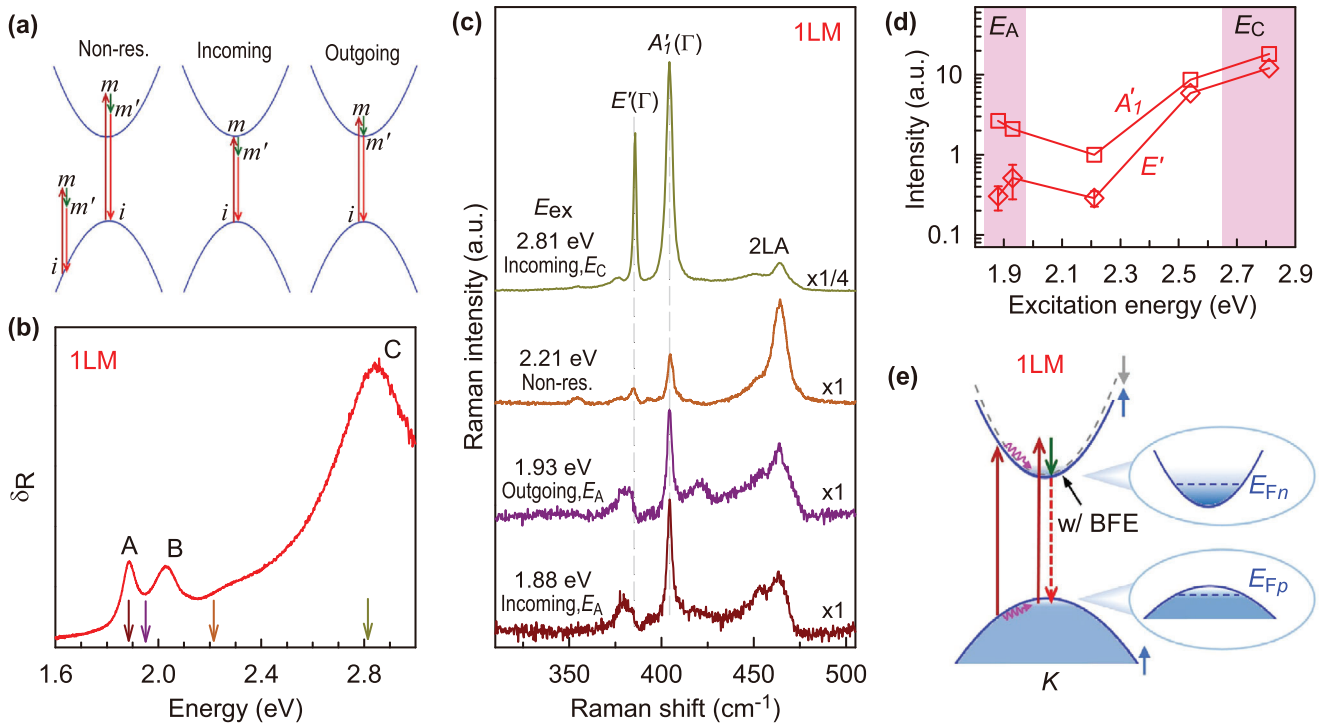

Figure 1. a) First-order Raman scattering under the non-resonance (non-res.), incoming and outgoing resonance conditions. b) Differential reflectance spectrum of 1LM. c) The calibrated Raman spectra of 1LM on quartz under different excitation conditions. d) The calibrated $I(A_1')$, $I(E')$ of 1LM on quartz under different excitation conditions. The Raman intensities are normalized to the $I(A_1')$ obtained under E_{ex} = 2.21 eV. e) Schematic of the band structure at the band edges located at the ***K*** point for 1LM. The BFE near the CBM and VBM is illustrated in the inset.

from photoexcited carrier accumulation at the valence band maximum (VBM) and conduction band minimum (CBM). However, the suppressed resonant Raman intensity can be recovered in van der waals heterostructures (vdWHs) constructed by 1LM and graphene flakes, where interfacial charge transfer provides a nonradiative relaxation (NrR) channel to mitigate the BFE. Similarly, in multilayer MoS_2, partial recovery of $I(A_1')$ occurs due to an additional NrR channel of intervalley scattering. These findings advance the understanding of RRS in low-dimensional semiconductors, where BFE and NrR of photoexcited carriers play critical roles.

2. Results and Discussion

We first compare Raman spectra of 1LM under different excitation conditions. The A, B, and C excitonic peaks were identified from the differential reflectance spectra of 1LM on quartz substrate in Figure 1b.[19] Four E_{ex} were chosen to measure the Raman spectra of 1LM (Figure 1c) in the incoming (E_{ex} = 1.88 eV) and outgoing (E_{ex} = 1.93 eV) resonance with E_A, in the incoming resonance with E_C (E_{ex} = 2.81 eV), and under the non-resonance condition (E_{ex} = 2.21 eV), as marked in Figure 1b. The Raman intensity of A_3 mode of quartz at ≈465 cm^{-1} is used to calibrate $I(A_1')$ and $I(E')$ to eliminate the different efficiencies of Raman system at different E_{ex}. The results show that $I(A_1')$ and $I(E')$ in 1LM are extremely weak when E_{ex} matches E_A, which are only about twice as much as those under the non-resonance condition and one-tenth of those in the incoming resonance with E_C, as summarized in Figure 1d. Notably, this observation in 1LM completely differs from the case of monolayer WS_2, e.g., $I(A_1')$ exhibits significant enhancement when E_{ex} aligns with E_A in monolayer WS_2, even about twice that in the resonance with its E_C.[12] Therefore, the experimental results indicate that resonant Raman intensity of 1LM is significantly quenched when E_{ex} matches its E_A.

In the time-dependent perturbation theory of Raman scattering process, the peak intensity of the phonon mode in Raman spectroscopy is directly correlated with electron-phonon coupling strength. The weak $I(A_1')$ and $I(E')$ in 1LM under the resonance with E_A may indicate that the electron-phonon coupling strength decreases with a decreasing number of atomic layers of atomically thin MoS_2 flakes.[11,20,21] However, this contradicts the conventional expectation, as the electron-phonon coupling strength is expected to be stronger in low-dimensional systems due to the quantum confinement effect.[22] Furthermore, the high density of states at the band edge of 1LM should also provide favorable conditions to enhance $I(A_1')$ and $I(E')$. This suggests an underlying mechanism responsible for the anomalous intensity quenching. Elucidating its origin in 1LM is crucial for understanding this anomalous RRS phenomena.

The RRS process is intricately linked with transitions between two real electronic states, so the observed anomalous weak Raman intensity of 1LM in the resonance with its E_A should be correlated with its band structure. For example, when E_{ex} is higher than E_A, as the intraband decay of photoexcited carriers occurs much faster than the interband radiative recombination

© 2025 Wiley-VCH GmbH

in 1LM,[23,24] the photoexcited electrons and holes tend to accumulate at the CBM and VBM, which is known as BFE, as schematized in Figure 1e for the case of outgoing resonance with its E_A. The BFE can also occur in the incoming resonance with E_A of 1LM due to the presence of thermal fluctuations. Phenomenally, the incoming and outgoing RRS pathways should be blocked by the BFE, as illustrated in Figure 1e. This should result in the anomalous intensity quenching of $I(A_1')$ and $I(E')$ in 1LM when E_{ex} is in resonance with its E_A.

Notably, in addition to the direct bandgap characteristic of 1LM, the interplay between inversion asymmetry and spin-orbit interaction gives rise to a large spin-orbit splitting between the two highest valence bands and a small splitting between the two lowest conduction bands, in which the latter results in dark-bright exciton splitting.[25,26] In the single-particle picture, spin ordering of the lowest energy single-particle electron-hole transitions renders them still bright.[27] However, in the exciton picture, the theory revealed that the actual ground excitonic state is dark, which is attributed to the different masses of spin-up and spin-down electrons in the conduction band and the repulsive electron-hole exchange interaction.[27] This has been confirmed by the subtle optical features of the high-quality 1LM encapsulated in hBN flakes under low-temperature and strong magnetic field conditions.[28,29] In this study, we primarily investigate the RRS in uncapped 1LM at room temperature. Given the relatively small energy splitting (≈14 meV) between the lowest dark and bright exciton bands in 1LM compared to the thermal fluctuation energy (≈26 meV at 300 K), the interband non-radiative relaxation between these excitonic states is not particularly pronounced. Consequently, the BFE of photoexcited carriers can occur under the resonance excitation condition at room temperature, which will be fully discussed in the following. To facilitate subsequent discussion of the different NrR channels of photogenerated carriers within atomically thin MoS_2 and between adjacent constituents of vdWH, the single-particle band structure of 1LM is employed during the result analysis. This approach provides a clear framework for understanding carrier dynamics while remaining consistent with the room-temperature experimental conditions.

To verify the proposed explanation, the most straightforward approach is to mitigate the BFE effect and reactivate the A exciton related RRS pathway, then examine whether the resonant Raman intensity is enhanced. The vdWH constructed by 1LM and four-layer graphene (4LG) (see Section SI, Supporting Information), i.e., 1LM/4LG vdWH, is an ideal platform for studying this issue. In **Figure 2**a, we compare the Raman spectra of 1LM and 1LM/4LG on 90 nm SiO_2/Si substrate obtained under different E_{ex}, including E_{ex} = 2.81 eV (incoming resonance with E_C), 2.21 eV (non-resonance condition), 1.93 eV (outgoing resonance with E_A), 1.91 eV (incoming and outgoing resonance with E_A), and 1.88 eV (incoming resonance with E_A). The results show that $I(A_1')$ and $I(E')$ of the 1LM constituent in 1LM/4LG vdWH are comparable with these in standalone 1LM under E_C resonance condition or non-resonance condition. However, we discover that $I(A_1')$ and $I(E')$ of the 1LM constituent in 1LM/4LG vdWH are dramatically enhanced when E_{ex} is in resonance with the A exciton of 1LM, even around five times those in the incoming resonance with the C exciton of 1LM, as shown in Figure 2a. We also observe a slight blueshift of the A_1' mode in the vdWH compared

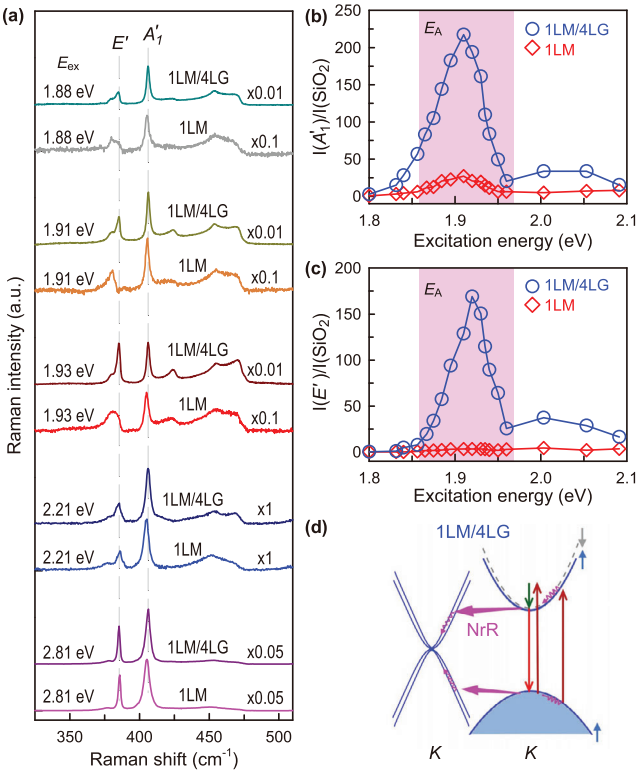

Figure 2. a) The calibrated Raman spectra of 1LM and 1LM/4LG on 90nm SiO_2/Si substrate under different excitation conditions. b) The resonant excitation profiles of the A_1' mode in 1LM and 1LM/4LG. c) The resonant excitation profiles of the E' mode in 1LM and 1LM/4LG. The Raman intensity is normalized by the A_3 mode of quartz at 465 cm^{-1} to eliminate the different efficiencies of charge-coupled device at different E_{ex}. d) Schematic of the band structure at the band edges of the ***K*** point for 1LM/4LG.

to the corresponding standalone MoS_2 flake. This feature originates from the interfacial coupling between MoS_2 and graphene constituents, which causes a perturbation to the A_1' mode of 1LM by its adjacent 4LG.[30]

Because the physisorbed molecules under ambient conditions may affect the physical properties of MoS_2, in order to eliminate the influence of ambient conditions on the experimental results, we compared the resonant Raman spectra of hBN-capped and uncapped 1LM and 1LM/4LG in the Section SII (Supporting Information). The corresponding results demonstrate that the spectra of uncapped 1LM (1LM/4LG) closely resemble that acquired in hBN-capped 1LM (1LM/4LG) at room temperature. This suggests that the uncapped 1LM in this work are not subjected to the photo-doping effects caused by the laser excitation under the ambient test condition. The absence of photo-doping effect in the Raman measurements can be attributed to the low excitation power (<150 μW) in the measurement, as the photo-doping effect usually occurs under high excitation powers.[31] Because the high-frequency intralayer modes are usually localized in the corresponding constituents of vdWHs,[32] the electron–phonon coupling strength of intralayer A_1' and E' modes would not show significant differences in 1LM and 1LM/4LG. The observed significant intensity quenching in 1LM and intensity recovery in

© 2025 Wiley-VCH GmbH

1LM/4LG of the A_1' and E' modes is a signature of a change between the A exciton related RRS pathways of 1LM and 1LM/4LG.

Remarkably, when the excitation profile of Raman intensity in the RRS exhibits a sharp feature, just a slight deviation of the E_{ex} near the peak of excitation profile should induce substantial variations in Raman intensity. This phenomenon is especially significant in the case of hBN-encapsulated 1LM at low temperature.[33] According to the PL peaks of 1LM and 1LM/4LG, their A excitons exhibit a small energy difference of ≈25 meV (see Section SI, Supporting Information) induced by their different dielectric environments. Thus, it is necessary to consider the difference in the resonant excitation conditions of standalone 1LM and 1LM/4LG and fully reveal the resonance behavior of their A_1' and E' modes. Here, 18 E_{ex} (from 1.80 to 2.09 eV) crossing E_A of both 1LM and 1LM/4LG are used to detect the resonance behavior of the two modes. Their normalized Raman intensities are shown in Figure 2b,c, which indicate that the A_1' (E') modes in both 1LM and 1LM/4LG exhibit a similar resonance excitation profile with slightly different positions at the maximum intensity. However, $I(A_1')$ and $I(E')$ in the 1LM/4LG are significantly stronger than those in the standalone 1LM when E_{ex} is close to E_A. Furthermore, in comparison to the sharp excitation profile in hBN-encapsulated 1LM at low temperature,[33] the resonance excitation profiles of A_1' (E') mode in both 1LM and 1LM/4LG are very broad (with a full width at half maximum exceeding 50 meV), which is much broader than the E_A difference (≈25 meV). This directly confirms that the difference in resonant Raman intensity between 1LM and 1LM/4LG does not originate from the difference in resonance excitation conditions. An underlying physical mechanism should drive the recovery of $I(A_1')$ and $I(E')$ in 1LM/4LG. In fact, in 1LM/4LG, interfacial charge transfer occurs between 1LM and 4LG constituents, which can be confirmed by the intensity quenching of PL peaks (see Section SI, Supporting Information). This could be a NrR channel to effectively mitigate the BFE of photoexcited carriers in 1LM constituent, which reactivates the corresponding RRS pathways associated with the A exciton and thus contributes to the recovery of $I(A_1')$ and $I(E')$ in 1LM/4LG, as shown in Figure 2d.

For a specific analysis, the quasi-Fermi levels of electrons (E_{Fn}) and holes (E_{Fp}) are commonly employed to assess the accumulation of photoexcited carriers in non-equilibrium conditions and are defined as[34]

$$E_{Fn} = E_{CBM} + k_B T \ln(n_e / N_{CBM})$$
$$E_{Fp} = E_{VBM} - k_B T \ln(n_p / N_{VBM}) \quad (1)$$

where E_{CBM} (E_{VBM}) is the energy of CBM (VBM), n_e (n_p) is the electron (hole) density, N_{CBM} (N_{VBM}) is the density of state at the CBM (VBM), k_B is the Boltzmann constant and T is the temperature. The photoexcited carriers accumulation will drive the E_{Fn} and E_{Fp} away from the CBM and VBM, respectively, and the BFE occurs. Due to the larger effective mass of the hole than that of the electron in TMDs, the VBM presents higher density of states N_{VBM}.[16] Thus, E_{Fn} deviates more significantly from the band-edge state than E_{Fp} in TMDs, which suggests that the BFE caused by photoexcited electrons is more evident than that caused by holes. According to the Equation (1), the BFE is sensitive to carrier density, which could be changed by varying the excitation power.[35] For a given T, n_e and n_p increases with excitation power. Consequently, E_{Fn} and E_{Fp} progressively shift away from the CBM and VBM, respectively, resulting in a more significant blocking of the RRS pathways as excitation power increases. Based on this analysis, the Raman intensity in resonance with the A exciton of 1LM is expected to reach a saturated value upon increasing excitation power. Indeed, the excitation power-dependent $I(A_1')$ in 1LM in the outgoing resonance with E_A shows nonlinear behavior and reaches a saturated value at excitation powers exceeding 50 μW, as depicted in **Figure 3a**. This confirms the BFE on blocking RRS pathway for quenched Raman intensity. In comparison with the case of 1LM, a linear excitation-power dependence of $I(A_1')$ in resonance with the A exciton of the 1LM constituent in 1LM/4LG can be observed in Figure 3b, which further confirms the assumption of BFE mitigation in 1LM/4LG. These analyses reveal that BFE is crucial for blocking RRS pathway. Furthermore, introducing NrR channel is an effective method to control RRS pathways and thus RRS intensity by manipulating the BFE of photoexcited carriers.

According to the Equation (1), E_{Fn} and E_{Fp} become more closer to the band edge with decreasing T, due to the reduced thermal fluctuation. Thus, BFE and the blocking of RRS pathway becomes less pronounced in standalone 1LM at lower T, resulting in stronger Raman intensity. This should result in smaller $I(A_1')$ ratio between 1LM/4LG and 1LM at lower T, as 1LM/4LG shows negligible BFE. To check the important role of BFE on blocking RRS pathways, we further measured the Raman spectra of standalone 1LM and 1LM/4LG in the outgoing resonance with the corresponding A exciton of 1LM at 300 and 4 K (Section SIII, Supporting Information), which shows smaller $I(A_1')$ ratio between 1LM/4LG and 1LM at 4 K than that at 300 K. This is in agreement with the above analysis, suggesting that the BFE is the main mechanism for RRS pathway blocking. Notably, considering that the physisorbed molecules under ambient conditions may affect the physical properties of uncapped samples, the experimental results at 300 and 4 K are both obtained in vacuum to eliminate the influence of ambient condition.

As the BFE is determined by the relaxation dynamics of photoexcited carriers at the CBM and VBM, we conducted a thorough investigation of the relaxation dynamics of photoexcited carriers related to the A exciton of 1LM and 1LM/4LG, by measuring the A-exciton bleach signal in the corresponding TA spectra (Figure 3c,d). The bleach signal originates from the photoexcited carriers accumulation at both CBM and VBM. In 1LM, the A-exciton bleach signal decays in tens of picoseconds with a fast process of ≈2.0 ps and a slow process of ≈24.1 ps, as shown in Figure 3e. The fast decay process results from charge transfer between 1LM and substrate and/or trapping of surface defect states, while the slow decay process is correlated with interband relaxation.[23,24] In contrast, in 1LM/4LG, the A-exciton bleach signal decays much faster in several picoseconds, with an ultra fast process of ≈0.6 ps and a slow process of ≈8.4 ps, as shown in Figure 3f. The ultrafast decay process can be attributed to the interfacial charge transfer between 1LM and 4LG, while the slow process is related to interband relaxation. The measurements in relaxation dynamics of photoexcited carriers suggest the interfacial charge transfer between 1LM and 4LG constituents of 1LM/4LG vdWH significantly shortens the lifetime of photoexcited carriers, which directly mitigates the BFE of photoexcited

© 2025 Wiley-VCH GmbH

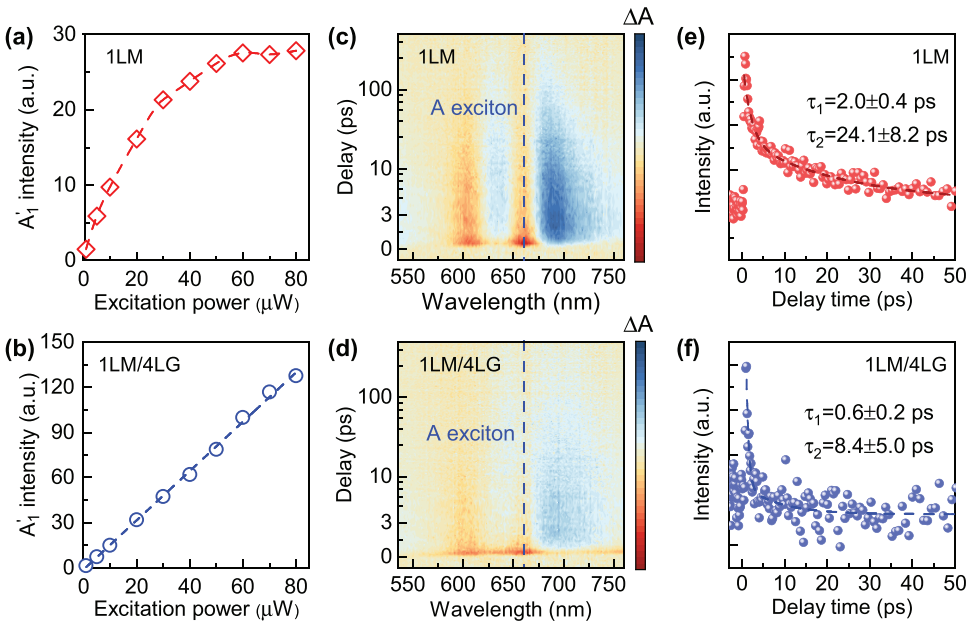

Figure 3. $I(A_1')$ in a) 1LM and b) 1LM/4LG under different excitation power. 2D pseudocolor plot of TA spectra in c) 1LM and d) 1LM/4LG under 1.93 eV excitation. Photoexcited carrier dynamics of the A exciton in e) 1LM and f) 1LM/4LG.

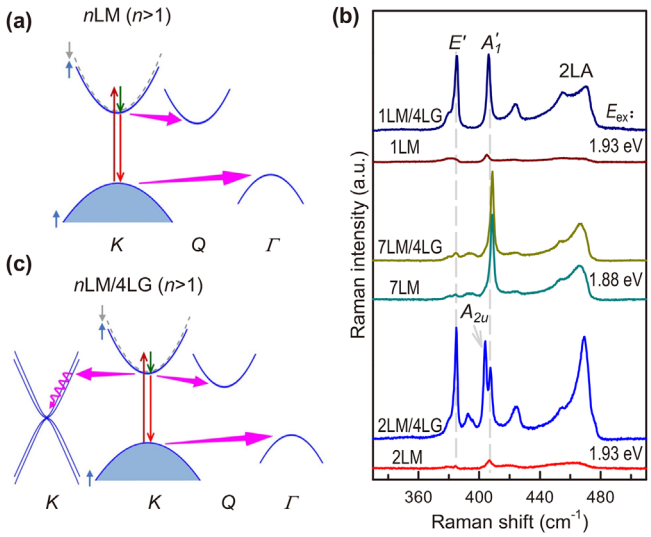

Figure 4. a) Schematic of the simplified band structure for *n*LM ($n > 1$). b) Raman spectra of 1LM, 1LM/4LG, 7LM, 7LM/4LG, 2LM, and 2LM/4LG obtained under outgoing resonance conditions with their corresponding A excitons. c) Schematic of the simplified band structure for *n*LM/4LG ($n > 1$).

carriers at both CBM and VBM and thus weakens RRS pathway blocking.

In TMDs, geometrical confinement effect leads to significant evolution of energy dispersion from monolayer thickness to bulk.[36] In constrast to 1LM with direct band structure,[37] multilayer MoS_2 with layer number n (nLM, $n > 1$) exhibits indirect band structure (**Figure** 4a). The CBM of nLM shifts from the ***K*** point to the ***Q*** point of the Brillouin zone, and the VBM of nLM shifts from the ***K*** point to the ***Γ*** point.[38] Consequently, intervalley scattering between ***K*** valley and ***Q*** (***Γ***) valley in nLM ($n > 1$) could be a NrR channel for the electrons (holes) in ***K*** valley. For simplicity, we use A_1' of 1LM to denote the corresponding modes in nLM ($n > 1$). Due to the mitigation of the BFE in nLM ($n > 1$), $I(A_1')$ of nLM ($n > 1$) should exhibit weaker quenching than 1LM when E_{ex} is in resonance with the corresponding A exciton. Indeed, $I(A_1')$ of 7LM does not exhibit obvious quenching when E_{ex} is in resonance with E_A, which is totally different from that in 1LM, as shown in Figure 4b. Notably, for the case of 2LM, $I(A_1')$ is extremely weak even in resonance with the A exciton, as depicted in Figure 4b. This can be ascribed to the evident BFE in 2LM, because the intervalley scattering cannot serve as an efficient NrR channel for photoexcited electrons at ***K*** valley due to the small energy difference between the CBM at the ***K*** and ***Q*** valleys.

When assembling nLM with 4LG together to form nLM/4LG vdWHs, both interfacial charge transfer and intervalley scattering can simultaneously present as NrR channels for photoexcited carriers, as demonstrated in Figure 4c. Figure 4b also shows Raman spectra of 1LM/4LG, 7LM/4LG and 2LM/4LG, in resonance with their corresponding A exciton, respectively. $I(A_1')$ in 7LM/4LG is almost equal to that in 7LM, indicating that the intervalley scattering is the main NrR channel to mitigate the BFE at the A exciton in 7LM/4LG vdWHs. While in 2LM/4LG, $I(A_1')$ exhibits a significant enhancement compared with that in 2LM, implying that the interfacial charge transfer is the dominant NrR channel to migrate BFE for the activation of RRS pathway in 2LM/4LG, in addition to the pristine NrR channel of intervalley scattering in 2LM.

To further confirm that the interfacial charge transfer between nLM and 4LG constituents is an efficient NrR channel to mitigate BFE of photoexcited carriers and activate RRS pathways in nLM/4LG, we inserted a 16L-hBN flake between 2LM and 4LG to form a 2LM/hBN/4LG vdWH. The layer number of the 16L-hBN is identified by the layer-breathing mode of 2LM/hBN/4LG

© 2025 Wiley-VCH GmbH

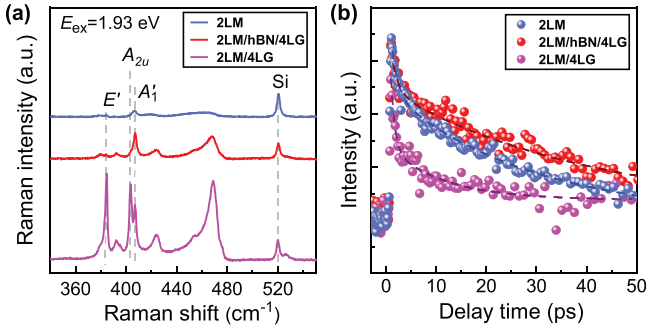

Figure 5. a) Raman spectra of 2LM, 2LM/4LG and 2LM/hBN/4LG. b) Photoexcited carrier dynamics of the A exciton in 2LM, 2LM/4LG and 2LM/hBN/4LG.

(see Section SV, Supporting Information) via cross-dimensional electron–phonon coupling effect.[13] Due to the wide bandgap of 16L-hBN, it can serve as a barrier layer to effectively block the interfacial charge transfer between the 2LM and 4LG constituents. Indeed, $I(A_1')$ in 2LM/hBN/4LG is obviously weaker than that in 2LM/4LG, but is slightly stronger than that in standalone 2LM, as shown in **Figure** 5a. This can be ascribed to the partial recovery of the BFE at the A exciton due to the blocking of interfacial charge transfer between 2LM and 4LG constituents by the 16L-hBN spacer layer, while the tunnelling effect through the hBN barrier and Förster resonance energy transfer between 2LM and 4LG constituents still result in the weaker BFE in 2LM/hBN/4LG relative to the case of standalone 2LM. The blocking of interfacial charge transfer between 2LM and 4LG constituents in 2LM/hBN/4LG can also be confirmed by the longer lifetime of photoexcited carriers in 2LM/hBN/4LG than that in 2LM/4LG and the similar lifetime of photoexcited carriers in 2LM/hBN/4LG and 2LM (Figure 5b).

Finally, gate-tunable resonant Raman spectroscopy of atomically thin MoS_2 can provide strong evidence for above analysis. Under the resonance condition with E_A, the Raman intensity of 2LM transistor with ionic gel gating is extremely weak when the gate voltage is positive.[39] When a negative gate voltage is applied, the resonant Raman intensity in 2LM can be gradually enhanced.[39] This result can be well understood by considering the enhancement or mitigation of BFE. Through applying positive or negative gate voltage, positively or negatively charged ions are driven to accumulate atop the sample to form electric double layer which then results in an increase or decrease of n_e in the sample. According to the Equation (1), the increase (decrease) of n_e is expected to enhance (mitigate) the BFE, and thus manipulate the resonant Raman intensity. Upon applying positive gate voltage, n_e of 2LM increases, which can enhance the BFE and thus induce significant quenching of resonant Raman intensity. When applying negative gate voltage, n_e of 2LM decreases, which is equivalent to mitigating the BFE. In this case, the A exciton related RRS pathway is activated and the resonant Raman intensity in 2LM can be recovered.

3. Conclusion

This work reports an anomalous quenching of $I(A_1')$ in 1LM when E_{ex} is in resonance with its E_A, e.g., $I(A_1')$ in 1LM is roughly one-tenth of its value under the resonance with E_C, while the corresponding $I(A_1')$ is twice that under its C-exciton resonance in monolayer WS_2. This unusual phenomenon in 1LM is attributed to the blocking of the corresponding Raman scattering pathway arising from the BFE of photoexcited carriers at the A exciton. This result is approved by the nonlinear excitation-power dependence of $I(A_1')$ in 1LM. Remarkably, the strongly quenched resonant Raman intensity can be recovered through manipulating BFE by introducing NrR channels for the photoexcited carriers, thereby reactivating the corresponding RRS pathway. In comparison with the standalone 1LM, the BFE is mitigated in nLM (n >1), 1LM-based and nLM-based vdWHs, leading to significant recovery of $I(A_1')$. The corresponding intensity recovery stems from the presence of additional NrR channels including interfacial charge transfer, intervalley scattering, carrier tunneling, and Förster resonance energy transfer. This work paves the way to optimize the sensitivity of Raman spectroscopy by engineering carrier relaxation dynamics to enhance RRS intensity, enabling insights into electronic transitions and electron–phonon coupling in low-dimensional semiconductors and related heterostructures.

4. Experimental Section

Sample Preparation: Atomically thin MoS_2 flakes were mechanically exfoliated from the corresponding bulk crystals onto polydimethylsiloxane (PDMS) sheets, while graphene flakes were exfoliated onto 90 nm SiO_2/Si substrates. The layer number of atomically thin graphene flakes were identified by analyzing the line shape of the 2D peak,[40] whereas the layer number of MoS_2 flakes were distinguished using peak positions of the interlayer phonons.[41] The vdWHs was constructed through the all-dry viscoelastic stamping method.[32,42] The TMD flakes on PDMS can be sequentially transferred onto graphene or 90 nm SiO_2/Si substrates in specific orders with the aid of an optical microscope and a nanomanipulator. All the fabricated samples were subjected to annealing under vacuum conditions (approximately 10^{-7} hpa) at 250 °C for 2 h to achieve a good interfacial coupling in vdWH. In the Section SI (Supporting Information), the optical image and photoluminescence mapping for 1LM, 1LM/4LG, 2LM and 2LM/4LG on 90 nm SiO_2/Si substrates were demonstrated to prove the high quality of the corresponding samples.

Raman Measurements: Raman spectra were measured under a backscattering configuration at 300 K with a Jobin Yvon HR800 Raman system equipped with a liquid-nitrogen-cooled charge-coupled device (CCD) and a 100× objective (numerical aperture = 0.90). 1800 and 2400 lines per mm gratings were used in the Raman measurements. The excitation energies were 2.81 eV from a HeCd laser, 2.33 eV from a diode-pumped-solid-state laser, 2.21 eV from a solid state single longitudinal mode laser, 1.96 eV from a HeNe laser and 1.80–2.09 eV from a C-wave GTR laser (HÜBNER Photonics GmbH). The Raman spectra at 4 K were measured in a helium-cooled cryostat (Montana Instruments), with Raman signal collected by a 50× objective (numerical aperture = 0.45).

Transient Absorption (TA) Spectra: Transient absorption (TA) spectroscopy conveys information about photoexcited carriers.[43] Microscopic TA measurements on TMD flakes and TMD/graphene vdWHs were performed with a custom-built microscopic system integrated into the HELIOS setup. Fundamental 800-nm pulses (1 kHz, 100 fs) from a Coherent Astrella regenerative amplifier were utilized to pump an optical parametric amplifier (Coherent, Opera Solo) to obtain a frequency-tunable pump beam. The probe beam was generated by focusing a small fraction of the fundamental 800-nm beam onto a sapphire plate. The probe wavelength ranges from 450 to 785 nm, with the E_{ex} in resonance with the A exciton of MoS_2. Both the pump and probe beams were focused onto the sample using a 20× objective. Reflected probe light was collected through the lens into a fiber, while the pump light was filtered out using a pair of crossed polarizer.

© 2025 Wiley-VCH GmbH

Supporting Information

Supporting Information is available from the Wiley Online Library or from the author.

Acknowledgements

The authors acknowledged the support from the National Key Research and Development Program of China (Grant No. 2023YFA1407000), the Strategic Priority Research Program of CAS (Grant No. XDB0460000), National Natural Science Foundation of China (Grant Nos. 12322401, 12127807, 12393832 and 62374158), Beijing Nova Program (Grant No. 20230484301), Youth Innovation Promotion Association, Chinese Academy of Sciences (No. 2023125), CAS Project for Young Scientists in Basic Research (YSBR-026).

Conflict of Interest

The authors declare no conflict of interests.

Data Availability Statement

The data that support the findings of this study are available from the corresponding author upon reasonable request.

Keywords

atomically thin semiconductors, band filling effect, non-radiative relaxation, resonance Raman scattering, Raman scattering pathway

Received: April 9, 2025
Revised: June 11, 2025
Published online: July 15, 2025

[1] M. Cardona, *Light Scattering in Solids I*, vol. *8*, Springer, Berlin, **1983**.
[2] X. Zhang, X.-F. Qiao, W. Shi, J.-B. Wu, D.-S. Jiang, P.-H. Tan, *Chem. Soc. Rev.* **2015**, *44*, 2757.
[3] G. S. N. Eliel, M. V. O. Moutinho, A. C. Gadelha, A. Righi, L. C. Campos, H. B. Ribeiro, P.-W. Chiu, K. Watanabe, T. Taniguchi, P. Puech, M. Paillet, T. Michel, P. Venezuela, M. A. Pimenta, *Nat. Commun.* **2018**, *9*, 1221.
[4] S. Li, E. Drueke, Z. Porter, W. Jin, Z. Lu, D. Smirnov, R. Merlin, S. D. Wilson, K. Sun, L. Zhao, *Phys. Rev. Lett.* **2020**, *125*, 087202.
[5] Q.-H. Tan, Y.-M. Li, J.-M. Lai, Y.-J. Sun, Z. Zhang, F. Song, C. Robert, X. Marie, W. Gao, P.-H. Tan, J. Zhang, *Nat. Commun.* **2023**, *14*, 88.
[6] R. Saito, M. Hofmann, G. Dresselhaus, A. Jorio, M. S. Dresselhaus, *Adv. Phys.* **2011**, *60*, 413.
[7] C. Thomsen, S. Reich, *Phys. Rev. Lett.* **2000**, *85*, 5214.
[8] P.-H. Tan, *Raman Spectroscopy of Two-Dimensional Materials*, Springer Singapore, Singapore, **2019**.
[9] J.-B. Wu, X. Zhang, M. Ijäs, W.-P. Han, X.-F. Qiao, X.-L. Li, D.-S. Jiang, A. C. Ferrari, P.-H. Tan, *Nat. Commun.* **2014**, *5*, 5309.
[10] C. Cong, T. Yu, *Nat. Commun.* **2014**, *5*, 4709.
[11] B. R. Carvalho, L. M. Malard, J. M. Alves, C. Fantini, M. A. Pimenta, *Phys. Rev. Lett.* **2015**, *114*, 136403.
[12] E. Del Corro, A. Botello-Méndez, Y. Gillet, A. L. Elias, H. Terrones, S. Feng, C. Fantini, D. Rhodes, N. Pradhan, L. Balicas, X. Gonze, J.-C. Charlier, M. Terrones, M. A. Pimenta, *Nano Lett.* **2016**, *16*, 2363.
[13] M.-L. Lin, Y. Zhou, J.-B. Wu, X. Cong, X.-L. Liu, J. Zhang, H. Li, W. Yao, P.-H. Tan, *Nat. Commun.* **2019**, *10*, 2419.
[14] G. Wang, A. Chernikov, M. M. Glazov, T. F. Heinz, X. Marie, T. Amand, B. Urbaszek, *Rev. Mod. Phys.* **2018**, *90*, 021001.
[15] Z. Y. Zhu, Y. C. Cheng, U. Schwingenschlögl, *Phys. Rev. B* **2011**, *84*, 153402.
[16] A. Ramasubramaniam, *Phys. Rev. B* **2012**, *86*, 115409.
[17] L. Sun, J. Yan, D. Zhan, L. Liu, H. Hu, H. Li, B. K. Tay, J.-L. Kuo, C.-C. Huang, D. W. Hewak, P. S. Lee, Z. X. Shen, *Phys. Rev. Lett.* **2013**, *111*, 126801.
[18] A. Carvalho, R. M. Ribeiro, A. H. Castro Neto, *Phys. Rev. B* **2013**, *88*, 115205.
[19] Y. Li, A. Chernikov, X. Zhang, A. Rigosi, H. M. Hill, A. M. van der Zande, D. A. Chenet, E.-M. Shih, J. Hone, T. F. Heinz, *Phys. Rev. B* **2014**, *90*, 205422.
[20] H. Li, Q. Zhang, C. C. R. Yap, B. K. Tay, T. H. T. Edwin, A. Olivier, D. Baillargeat, *Adv. Funct. Mater.* **2012**, *22*, 1385.
[21] N. Scheuschner, O. Ochedowski, M. Schleberger, J. Maultzsch, *Phys. Status Solidi B* **2012**, *249*, 2644.
[22] E. R. Kennehan, G. S. Doucette, A. R. Marshall, C. Grieco, K. T. Munson, M. C. Beard, J. B. Asbury, *ACS Nano* **2018**, *12*, 6263.
[23] H. Shi, R. Yan, S. Bertolazzi, J. Brivio, B. Gao, A. Kis, D. Jena, H. G. Xing, L. Huang, *ACS Nano* **2013**, *7*, 1072.
[24] L. Gao, Z. Hu, J. Lu, H. Liu, Z. Ni, *Phys. Chem. Chem. Phys.* **2021**, *23*, 8222.
[25] H. Yu, X. Cui, X. Xu, W. Yao, *Natl. Sci. Rev.* **2015**, *2*, 57.
[26] J. P. Echeverry, B. Urbaszek, T. Amand, X. Marie, I. C. Gerber, *Phys. Rev. B* **2016**, *93*, 121107.
[27] M. Bieniek, L. Szulakowska, P. Hawrylak, *Phys. Rev. B* **2020**, *101*, 125423.
[28] C. Robert, B. Han, P. Kapuscinski, A. Delhomme, C. Faugeras, T. Amand, M. R. Molas, M. Bartos, K. Watanabe, T. Taniguchi, B. Urbaszek, M. Potemski, X. Marie, *Nat. Commun.* **2020**, *11*, 4037.
[29] J. Jadczak, J. Kutrowska-Girzycka, M. Bieniek, T. Kazimierczuk, P. Kossacki, J. J. Schindler, J. Debus, K. Watanabe, T. Taniguchi, C. H. Ho, A. Wójs, P. Hawrylak, L. Bryja, *Nanotechnology* **2021**, *32*, 145717.
[30] K.-G. Zhou, F. Withers, Y. Cao, S. Hu, G. Yu, C. Casiraghi, *ACS Nano* **2014**, *8*, 9914.
[31] B. Miller, E. Parzinger, A. Vernickel, A. W. Holleitner, U. Wurstbauer, *Appl. Phys. Lett.* **2015**, *106*, 122103.
[32] H. Wu, M.-L. Lin, Y.-C. Leng, X. Chen, Y. Zhou, J. Zhang, P.-H. Tan, *npj 2D Mater. Appl.* **2022**, *6*, 87.
[33] M. Zinkiewicz, M. Grzeszczyk, T. Kazimierczuk, M. Bartos, K. Nogajewski, W. Pacuski, K. Watanabe, T. Taniguchi, A. Wysmołek, P. Kossacki, M. Potemski, A. Babiński, M. R. Molas, *npj 2D Mater. Appl.* **2024**, *8*, 2.
[34] M. Grundmann, *The Physics of Semiconductors*, Graduate Texts in Physics. Springer International Publishing, Cham, **2021**.
[35] S. Raymond, S. Fafard, P. J. Poole, A. Wojs, P. Hawrylak, S. Charbonneau, D. Leonard, R. Leon, P. M. Petroff, J. L. Merz, *Phys. Rev. B* **1996**, *54*, 11548.
[36] W.-J. Zhao, Z. Ghorannevis, L. Chu, M. Toh, C. Kloc, P.-H. Tan, G. Eda, *ACS Nano* **2013**, *7*, 791.
[37] K. F. Mak, C. Lee, J. Hone, J. Shan, T. F. Heinz, *Phys. Rev. Lett.* **2010**, *105*, 136805.
[38] A. Splendiani, L. Sun, Y. Zhang, T. Li, J. Kim, C.-Y. Chim, G. Galli, F. Wang, *Nano Lett.* **2010**, *10*, 1271.
[39] X. Lu, M. I. B. Utama, X. Wang, W. Xu, W. Zhao, M. H. S. Owen, Q. Xiong, *Small* **2017**, *13*, 1701039.
[40] W. J. Zhao, P. H. Tan, J. Zhang, J. A. Liu, *Phys. Rev. B* **2010**, *82*, 245423.
[41] X. Zhang, W. P. Han, J. B. Wu, S. Milana, Y. Lu, Q. Q. Li, A. C. Ferrari, P. H. Tan, *Phys. Rev. B* **2013**, *87*, 115413.
[42] A. Castellanos-Gomez, M. Buscema, R. Molenaar, V. Singh, L. Janssen, H. S. J. Van Der Zant, G. A. Steele, *2D Mater.* **2014**, *1*, 011002.
[43] F. Ceballos, H. Zhao, *Adv. Funct. Mater.* **2017**, *27*, 1604509.

© 2025 Wiley-VCH GmbH

Supporting Information
Anomalous Intensity Quenching of Resonant Raman Scattering in Atomically Thin MoS_2

Rui Mei, Yang-Guang Zhong, Jia-Liang Xie, Jiang-Bin Wu, Wen-Na Du, Xin-Hui Zhang, Xin-Feng Liu, Miao-Ling Lin, Ping-Heng Tan**

R. Mei, J.-L. Xie, J.-B. Wu, X.-H. Zhang, M.-L. Lin, P.-H. Tan
State Key Laboratory of Semiconductor Physics and Chip Technologies,
Institute of Semiconductors, Chinese Academy of Sciences,
Beijing 100083, China
Email Address: linmiaoling@semi.ac.cn, phtan@semi.ac.cn
R. Mei, J.-L. Xie, J.-B. Wu, X.-H. Zhang, M.-L. Lin, P.-H. Tan
Center of Materials Science and Optoelectronics Engineering,
University of Chinese Academy of Sciences,
Beijing 100049, China
Y.-G. Zhong, W.-N. Du, X.-F. Liu
CAS Key Laboratory of Standardization and Measurement for Nano-technology,
National Center for Nanoscience and Technology,
Beijing 100190, China.

Section I: Optical image and photoluminescence (PL) mapping for our sample

In **Figures** S1a and S1b, we demonstrate the optical image and PL mapping for 1LM, 1LM/4LG, 2LM and 2LM/4LG on 90 nm SiO_2/Si substrate. The PL peaks of 1LM/4LG and 2LM/4LG vdWHs are uniformly quenched in their corresponding regions, which indicates a good interfacial coupling quality over a large area. In Figure S1c, we demonstrate the PL quenching of 1LM/4LG and 2LM/4LG vdWHs.

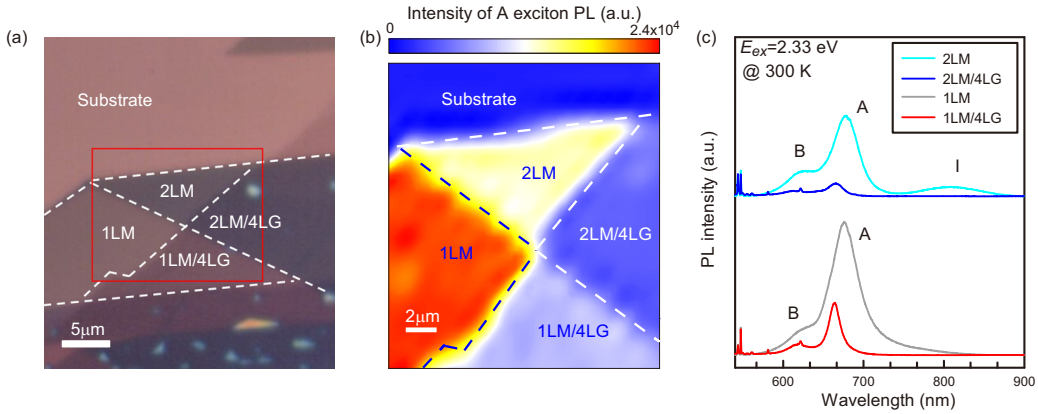

Figure S1: Optical image a) and PL mapping b) for 1LM, 1LM/4LG, 2LM and 2LM/4LG on 90 nm SiO_2/Si substrate. c) PL spectra of 1LM, 1LM/4LG, 2LM and 2LM/4LG.

Section II: Resonant Raman spectra of hBN-capped and ucapped 1LM and 1LM/4LG

In order to eliminate the influence of ambient conditions on the experimental results, we compared the resonant Raman spectra of hBN-capped and uncapped 1LM and 1LM/4LG. **Figure** S2a presents the optical image of our sample which simultaneously includes different regions. Raman spectra of hBN-capped 1LM and uncapped 1LM obtained under outgoing resonance condition with A exciton are compared in Figure S2b. The hBN-capped 1LM exhibits the same Raman intensity quenching as the uncapped 1LM. Moreover, the quenched Raman intensity is recovered in both hBN-capped 1LM/4LG and uncapped 1LM/4LG, as shown in Figure S2c. Based on these, the experimental results obtained in ambient condition are similar to those obtained in hBN-capped ones. This suggests that the uncapped 1LM in this work are not subjected to the photo-doping effects caused by the laser excitation under the ambient test condition.

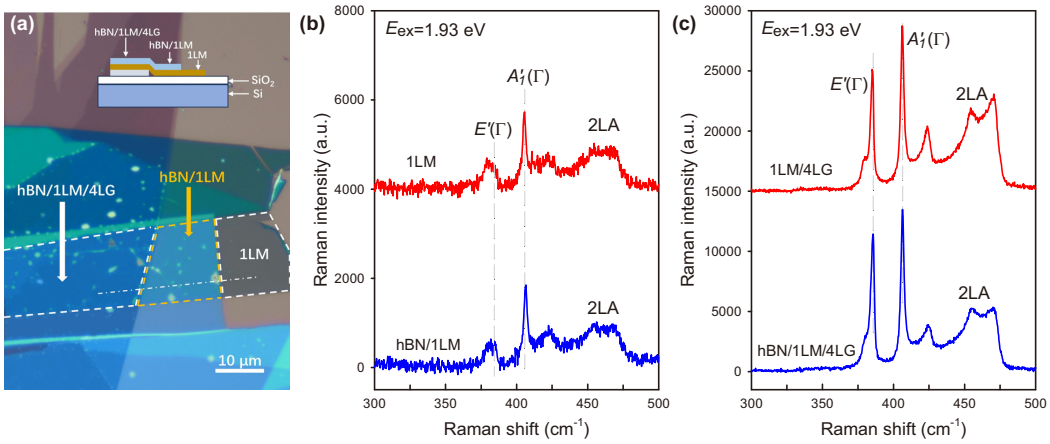

Figure S2: a) Optical image for hBN-capped 1LM, hBN-capped 1LM/4LG and uncapped 1LM. The inset shows the cross-section of the sample at the position indicated by the white dash-dotted line. b) Raman spectra of hBN-capped 1LM and uncapped 1LM obtained under outgoing resonance condition with A exciton. c) Raman spectra of hBN-capped 1LM/4LG and uncapped 1LM/4LG obtained under outgoing resonance condition with A exciton.

Section III: Temperature-dependent Raman spectra of 1LM amd 1LM/4LG

Figures S3a and S3b present the Raman spectra of 1LM and 1LM/4LG in the outgoing resonance with E_{A} at 300 and 4 K in vacuum, respectively, showing that the $I(\mathrm{A}_1^{'})$ ratio between 1LM/4LG and 1LM at 300 K is obviously larger than that at 4 K, as shown in Figure S3c. This behavior arises from the temperature-dependence of BFE. In comparison to the case at 300 K, E_{Fn} and E_{Fp} are closer to the band edge at 4 K due to the reduced thermal fluctuation, as depicted in Figure S3d. Consequently, the BFE of 1LM at 4 K is weakened relative to the case at 300 K, which then results in slightly weaker blocking of Raman scattering pathways in 1LM and accounts for the smaller $I(\mathrm{A}_1^{'})$ ratio between 1LM/4LG and 1LM at 4 K.

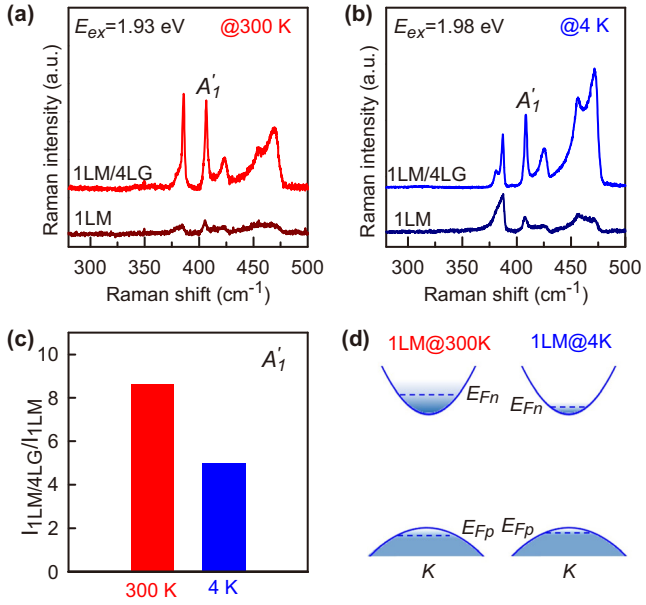

Figure S3: a) Raman spectra of 1LM and 1LM/4LG under 1.93 eV excitation at 300 K in vacuum. b) Raman spectra of 1LM and 1LM/4LG under 1.98 eV excitation at 4 K in vacuum. c) $I(\mathrm{A}_1^{'})$ ratio between 1LM/4LG and 1LM at 300 K (red) and 4 K (blue). d) Comparison of BFE at 300 K and 4 K.

Section IV: Differential reflectance spectra of 1LM, 2LM and 7LM

Figure S4 shows the differential reflectance spectra of 1LM, 2LM and 7LM, in which excitonic peaks A, B and C can be found.[1] Based on the result, the outgoing resonance conditions with E_A in 1LM, 2LM and 7LM can be determined (as marked in Figure S4).

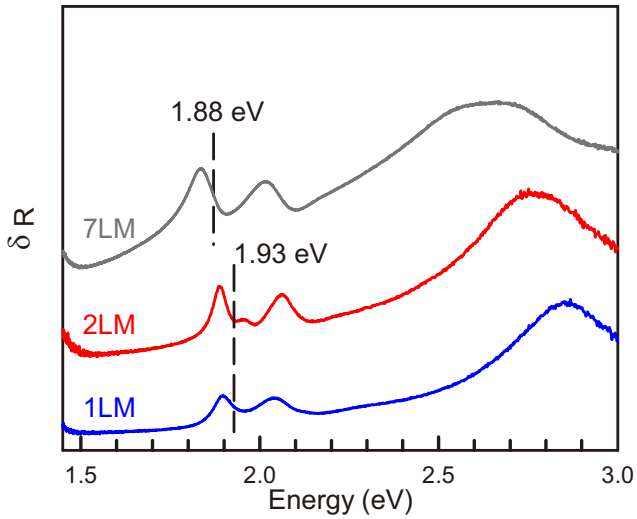

Figure S4: Differential reflectance spectra of 1LM, 2LM and 7LM on quartz substrates.

Section V: The determination of the layer number of hBN flake based on the cross-dimensional electron-phonon coupling

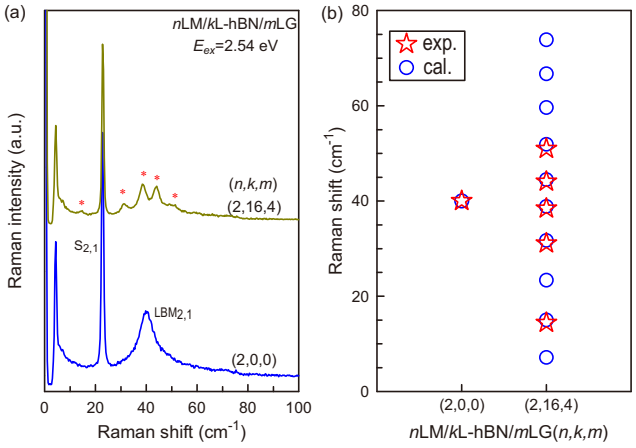

Figure S5: a) Low-frequency Raman spectra of 2LM and 2LM/16L-hBN/4LG. b) Experimentally observed LBMs frequencies (red star) and calculated LBMs frequencies of 2LM and 2LM/16L-hBN/4LG (blue circle).

Accurately identifying the layer number of hBN constituent in 2LM/hBN/4LG vdWH is important. Interlayer phonon modes including shear (S) mode and layer-breathing mode (LBM) have been widely used to identify the layer number of two-dimensional materials, which usually emerge in the low-frequency region (<150 cm^{-1}) of Raman spectra.[2] For an in-plane isotropic two-dimensional material flake with N rigid layers, there are N-1 degenerate S modes and N-1 LBMs, which are denoted as $S_{N,N-i}$ and $LBM_{N,N-i}$ (i = 1, 2, ..., N-1), respectively, where the $S_{N,1}$ ($LBM_{N,1}$) (*i.e.*, $i = N$-1) is the one with the highest frequency and $S_{N,N-1}$ ($LBM_{N,N-1}$) (*i.e.*, $i = 1$) is the one with the lowest frequency. For example, in 2LM, the S mode ($S_{2,1}$) is observed at 22.5 cm^{-1}, and the LBM ($LBM_{2,1}$) is observed at 40 cm^{-1}, as shown in **Figure** S5a. However, it is difficult to directly identify the layer number of hBN flake by its intrinsic low-frequency Raman spectrum, because the standalone hBN flake exhibits no observable LBMs due to its extremely weak electron-phonon coupling strength when subjected to visible laser excitation.[3]

The cross-dimensional electron-phonon coupling effect[3] provides a strategy to identify the layer number of hBN constituent via measuring the LBMs frequencies of 2LM/hBN/4LG vdWH. Here, a series of LBMs can be experimentally observed in the ternary 2LM/hBN/4LG vdWH, as shown in Figure S5a. The experimentally observed LBMs frequencies are summarized in Figure S5b. Notably, the linear chain model has been widely used to predict the frequencies of the S modes and LBMs in two-dimensional materials and vdWHs.[2–4] Based on this model, we can calculate all the LBM frequencies of the corresponding ternary vdWH, and thus determine the layer number of hBN flake. When we consider the structure as 2LM/16L-hBN/4LG, the calculated results are in agreement with the experimental ones, as shown in Figure S5b.

References

[1] Y. Li, A. Chernikov, X. Zhang, A. Rigosi, H. M. Hill, A. M. van der Zande, D. A. Chenet, E.-M. Shih, J. Hone, T. F. Heinz, Measurement of the optical dielectric function of monolayer transition-metal dichalcogenides: MoS_2 , $MoSe_2$, WS_2, and WSe_2, *Phys. Rev. B* **2014**, *90*, 205422.

[2] X. Zhang, W. P. Han, J. B. Wu, S. Milana, Y. Lu, Q. Q. Li, A. C. Ferrari, P. H. Tan, Raman spectroscopy of shear and layer breathing modes in multilayer MoS_2, *Phys. Rev. B* **2013**, *87*, 115413.

[3] M.-L. Lin, Y. Zhou, J.-B. Wu, X. Cong, X.-L. Liu, J. Zhang, H. Li, W. Yao, P.-H. Tan, Cross-dimensional electron-phonon coupling in van der waals heterostructures, *Nat. Commun.* **2019**, *10*, 2419.

[4] P. H. Tan, W. P. Han, W. J. Zhao, Z. H. Wu, K. Chang, H. Wang, Y. F. Wang, N. Bonini, N. Marzari, N. Pugno, G. Savini, A. Lombardo, A. C. Ferrari, The shear mode of multilayer graphene, *Nat. Mater.* **2012**, *11*, 294.